



Publication Year	2020
Acceptance in OA	2025-03-17T13:11:45Z
Title	The baryon density of the Universe from an improved rate of deuterium burning
Authors	Mossa, V., Stöckel, K., Cavanna, F., Ferraro, F., Aliotta, M., Barile, F., Bemmerer, D., Best, A., Boeltzig, A., Brogini, C., Bruno, C. G., Caciolli, A., Chillery, T., Ciani, G. F., Corvisiero, P., Csedreki, L., Davinson, T., Depalo, R., Di Leva, A., Elekes, Z., Fiore, E. M., Formicola, A., Fülöp, Zs., Gervino, G., Guglielmetti, A., Gustavino, C., Gyürky, G., Imbriani, G., Junker, M., Kievsky, A., Kochanek, I., Lugaro, M., Marcucci, L. E., Mangano, G., Marigo, P., Masha, E., Menegazzo, R., Pantaleo, F. R., Patichio, V., Perrino, R., Piatti, D., Pisanti, O., Prati, P., Schiavulli, L., STRANIERO, Oscar, Szücs, T., Takács, M. P., Trezzi, D., Viviani, M., Zavatarelli, S.
Publisher's version (DOI)	10.1038/s41586-020-2878-4
Handle	http://hdl.handle.net/20.500.12386/36851
Journal	NATURE
Volume	587

The baryon density of the Universe from an improved rate of deuterium burning

V. Mossa¹, K. Stöckel^{2,3}, F. Cavanna^{4§}, F. Ferraro^{4,5}, M. Aliotta⁶, F. Barile¹, D. Bemmerer², A. Best⁷, A. Boeltzig^{8,9}, C. Brogгинi¹⁰, C.G. Bruno⁶, A. Cacioli^{10,11}, T. Chillery⁶, G.F. Ciani^{8,9}, P. Corvisiero^{4,5}, L. Csedreki^{8,9}, T. Davinson⁶, R. Depalo¹⁰, A. Di Leva⁷, Z. Elekes¹², E.M. Fiore^{1,13}, A. Formicola⁹, Zs. Fülöp¹², G. Gervino¹⁴, A. Guglielmetti¹⁵, C. Gustavino¹⁶, G. Gyürky¹², A. Kievsky¹⁷, G. Imbriani⁷, M. Junker⁹, I. Kochanek⁹, M. Lugaro^{18,19}, L.E. Marcucci^{17,20}, G. Mangano⁷, P. Marigo^{10,11}, E. Masha¹⁵, R. Menegazzo¹⁰, F.R. Pantaleo^{1,21}, V. Patricchio¹, R. Perrino^{1†}, D. Piatti¹⁰, O. Pisanti⁷, P. Prati^{4,5}, L. Schiavulli^{1,13}, O. Straniero^{9,22}, T. Szücs², M. P. Takács^{2,3}, D. Trezzi¹⁵, M. Viviani¹⁷, S. Zavatarelli⁴

November 24, 2020

¹*INFN, Sezione di Bari, via E. Orabona 4, 70125 Bari, Italy*

²*Helmholtz-Zentrum Dresden-Rossendorf, Bautzner Landstraße 400, 01328 Dresden, Germany*

³*Technische Universität Dresden, Zellescher Weg 19, 01069 Dresden, Germany*

⁴*INFN, Sezione di Genova, Via Dodecaneso 33, 16146 Genova, Italy*

⁵*Università degli Studi di Genova, Via Dodecaneso 33, 16146 Genova, Italy*

⁶*SUPA, School of Physics and Astrophysics, University of Edinburgh, Peter Guthrie Tait Road, EH9 3FD Edinburgh, United Kingdom*

⁷*Università degli Studi di Napoli “Federico II”, and INFN, Sezione di Napoli, Via Cintia 21, 80126*

[§]Permanent Address: INFN, Sezione di Torino, Via P. Giuria 1, 10125 Torino, Italy

[†]Permanent Address: INFN Sezione di Lecce, Via per Arnesano, 73100 Lecce, Italy

20 *Napoli, Italy*

21 ⁸*Gran Sasso Science Institute, Viale F. Crispi 7, 67100 L'Aquila, Italy*

22 ⁹*INFN, Laboratori Nazionali del Gran Sasso (LNGS), Via G. Acitelli 22, 67100 Assergi, Italy*

23 ¹⁰*INFN, Sezione di Padova, Via F. Marzolo 8, 35131 Padova, Italy*

24 ¹¹*Università degli Studi di Padova, Via F. Marzolo 8, 35131 Padova, Italy*

25 ¹²*Institute for Nuclear Research (Atomki), PO Box 51, 4001 Debrecen, Hungary*

26 ¹³*Università degli Studi di Bari, Dipartimento Interateneo di Fisica, Via G. Amendola 173, 70126*

27 *Bari, Italy*

28 ¹⁴*Università degli Studi di Torino and INFN, Sezione di Torino, Via P. Giuria 1, 10125 Torino,*

29 *Italy*

30 ¹⁵*Università degli Studi di Milano and INFN, Sezione di Milano, Via G. Celoria 16, 20133 Milano,*

31 *Italy*

32 ¹⁶*INFN, Sezione di Roma, Piazzale A. Moro 2, 00185 Roma, Italy*

33 ¹⁷*INFN, Sezione di Pisa, Largo B. Pontecorvo 3, 56127 Pisa, Italy*

34 ¹⁸*Konkoly Observatory, Research Centre for Astronomy and Earth Sciences, MTA Centre for Ex-*

35 *cellence, Konkoly Thege Miklos 15-17, H-1121 Budapest, Hungary*

36 ¹⁹*ELTE Eötvös Loránd University, Institute of Physics, Budapest 1117, Pázmány Péter sétány 1/A,*

37 *Hungary*

38 ²⁰*Università degli Studi di Pisa, Dipartimento di Fisica "E. Fermi", Largo B. Pontecorvo 3, 56127*

39 *Pisa, Italy*

40 ²¹*Politecnico di Bari, Dipartimento Interateneo di Fisica, Via G. Amendola 173, 70126 Bari, Italy*

41 ²²INAF Osservatorio Astronomico d'Abruzzo, Via Mentore Maggini, 64100 Teramo, Italy

42 **Among the light elements produced during Big Bang Nucleosynthesis^{1,2} (BBN), deuterium**
43 **is an excellent indicator of cosmological parameters because its abundance is highly sensi-**
44 **tive to the primordial baryon density and also depends on the number of neutrino species**
45 **permeating the early Universe. While astronomical observations of primordial deuterium**
46 **abundance have reached percent accuracy³, theoretical predictions⁴⁻⁶ based on BBN are**
47 **hampered by large uncertainties on the cross section of the deuterium burning $D(p,\gamma)^3\text{He}$**
48 **process. Here we show that our improved cross sections finally allow for BBN estimates of**
49 **the baryon density at the 1.6% level, in excellent agreement with a recent analysis of the**
50 **Cosmic Microwave Background⁷. Improved cross-section data were obtained by exploit-**
51 **ing the negligible cosmic-ray background deep underground at the Laboratory for Under-**
52 **ground Nuclear Astrophysics (LUNA) of the Laboratori Nazionali del Gran Sasso (Italy)^{8,9}.**
53 **We bombarded a high-purity deuterium gas target¹⁰ with an intense proton beam from the**
54 **LUNA 400 kV accelerator¹¹ and detected the γ rays from the nuclear reaction under study**
55 **with a high-purity germanium detector. Our experimental results settle the most uncertain**
56 **nuclear physics input to BBN calculations and substantially improve the reliability of using**
57 **primordial abundances as probes of the physics of the early Universe.**

58 Light elements were produced in the first few minutes of the Universe through a sequence
59 of nuclear reactions known as Big Bang Nucleosynthesis (BBN)^{1,2}. The theoretical description of
60 BBN is based on the standard cosmological model (hereafter the “ Λ CDM model”²), which assumes
61 a homogeneous and isotropic universe governed by general relativity and by the Standard Model of

62 particle physics. Under these assumptions, BBN predicts the abundances of primordial nuclides,
63 mainly ^2H (hereafter D), ^3He , ^4He , and ^7Li , as a function of one parameter only, the density of
64 ordinary matter, or baryon density, $\Omega_b h^2$ (see Fields *et al.*¹² for a recent review). Therefore, a
65 comparison between the observed primordial abundances and those predicted by the BBN can be
66 used to constrain this fundamental quantity. Yet an independent evaluation of $\Omega_b h^2$ can also be
67 obtained by measuring the anisotropies in the Cosmic Microwave Background (CMB), the relic
68 electromagnetic radiation left over from the Big Bang.

69 It should be noted that $\Omega_b h^2$ from the CMB reflects the baryon density of the Universe at
70 the re-combination epoch, some 380,000 years after the Big Bang. However, according to the
71 ΛCDM model, the baryon density can only vary as a result of the expansion of the Universe and
72 thus its present-day value inferred from either CMB and BBN should be the same. Therefore, the
73 evaluation of $\Omega_b h^2$ based on BBN alone is critical as it can either support the ΛCDM model or
74 point to new physics between the BBN and CMB epochs². We present a new evaluation of $\Omega_b h^2$
75 from BBN based on improved experimental nuclear physics inputs obtained at the Laboratory for
76 Underground Nuclear Astrophysics (LUNA)^{8,9} of the INFN Laboratori Nazionali del Gran Sasso
77 (Italy).

78 Of the elements produced during the BBN, deuterium (D) is an excellent indicator of cosmo-
79 logical parameters in the early Universe because its abundance is the most sensitive to the baryon
80 density $\Omega_b h^2$ and also depends on the radiation density, usually expressed in terms of the effec-
81 tive number N_{eff} of neutrino species². Since deuterium is almost exclusively produced during

82 BBN, and is only destroyed during stellar evolution, its primordial abundance can be obtained
 83 from astrophysical sites not affected by stellar evolution⁴. The best determination of the deu-
 84 terium abundance is presently obtained by analysing the light spectra of quasars crossing pristine
 85 gas clouds at high redshift. Recent astronomical observations³ have reached excellent precision
 86 and provide a weighted mean value of the primordial deuterium abundance relative to hydrogen,
 87 $(D/H)_{\text{obs}} = (2.527 \pm 0.030) \times 10^{-5}$, with a 1% uncertainty³ (hereafter, quoted errors are at 68%
 88 confidence level unless stated otherwise). By contrast, theoretical predictions of D/H based on
 89 BBN, $(D/H)_{\text{BBN}}$, are less clear: Coc *et al.*⁵ report a value in agreement with observations, but with
 90 a higher uncertainty, while Pitrou *et al.*⁴ report a value in tension with observations, albeit with
 91 a similar precision. Improving such predictions requires an accurate knowledge of the nuclear
 92 reaction rates involved in the synthesis of deuterium: specifically, production via the well-known
 93 $p(n,\gamma)D$ process, and destruction via the $D(d,n)^3\text{He}$, $D(d,p)^3\text{H}$, and $D(p,\gamma)^3\text{He}$ reactions. Of these,
 94 the $D(p,\gamma)^3\text{He}$ reaction⁴⁻⁶ carries the largest uncertainties because of insufficient experimental data
 95 at relevant BBN energies. While the $D(p,\gamma)^3\text{He}$ cross section, or equivalently its S factor (see
 96 Methods “ $D(p,\gamma)^3\text{He}$ cross-section measurements at LUNA”), is well known¹³ at low energies,
 97 $E \simeq 3 - 20$ keV (energies are in the centre of mass system unless stated otherwise), higher energy
 98 data¹⁴⁻¹⁷ are affected by systematic uncertainties of 9% or more. In addition, a recent *ab-initio*
 99 theoretical calculation¹⁸ disagrees at the level of 20-30% with a widely used S -factor best fit¹⁹ to
 100 selected data sets^{13-15,20} and at the level of $\sim 8\%$ with a fit by Iliadis *et al.*²¹. As a result, BBN
 101 predictions of primordial deuterium abundance remain unsatisfactory, which calls for improved
 102 measurements of the $D(p,\gamma)^3\text{He}$ reaction cross-section over a wide energy range^{3-6,12}.

103 The new measurement of the $D(p,\gamma)^3\text{He}$ cross section discussed in this paper was performed
 104 at the LUNA-400kV accelerator¹¹, a world-leading facility to study nuclear reactions at the low-
 105 est energies frontier of nuclear astrophysics. The million-fold reduction in cosmic-ray muons of
 106 the deep-underground location⁸ and a careful commissioning¹⁰ of the experimental setup aimed
 107 at minimising all sources of systematic errors have led to $D(p,\gamma)^3\text{He}$ cross-section data of un-
 108 precedented precision and with overall uncertainties below 3% over the measured energy region
 109 ($E = 32 - 263$ keV), relevant to BBN energies ($E = 30 - 300$ keV, see Methods). As shown
 110 in Figure 1, the new data represent a significant improvement compared to previous work^{14,15,17}.
 111 Our new S -factor best fit (red solid line) implies a destruction of deuterium that is faster com-
 112 pared to the best fit¹⁹ of previous experimental data (blue dashed curve), and slower compared to
 113 predictions based on the *ab-initio* calculation¹⁸ (black dotted curve).

114 To explore the impact of our $D(p,\gamma)^3\text{He}$ S -factor on the predicted primordial deuterium abun-
 115 dance, we used the second release²² of the numerical BBN code PArthENoPE. Under the assump-
 116 tion of the ΛCDM model, with^{23,24} $N_{\text{eff}} = 3.045$, we performed a Bayesian likelihood analysis
 117 (see Methods) to derive $\Omega_b h^2$ using the observed deuterium abundance, $(D/H)_{\text{obs}}$, and the the-
 118 oretical behaviour of $(D/H)_{\text{BBN}}$ (now including the new LUNA data). We obtain $\Omega_b h^2(\text{BBN}) =$
 119 0.02233 ± 0.00036 . As shown in Figure 2, this value is a factor of 2 more precise than that obtained
 120 using a previous S factor¹⁹ and now in much better agreement with the $\Omega_b h^2$ based on CMB data¹²
 121 (see values in Table 1). The use of BBN deuterium alone as a baryometer has now approached a
 122 precision comparable to that obtained from CMB analyses^{7,12}. The fact that the present-day values
 123 of $\Omega_b h^2(\text{BBN})$ and $\Omega_b h^2(\text{CMB})$ are fully consistent with each other (Table 1) offers evidence of

124 the validity of the Λ CDM model adopted here.

125 We note that if we use the baryon density provided by the PLANCK Collaboration⁷, we
126 derive a theoretical prediction on deuterium abundance $(D/H)_{\text{BBN}} = (2.52 \pm 0.03 \pm 0.06) \times 10^{-5}$,
127 in excellent agreement with astronomical observations³ $(D/H)_{\text{obs}} = (2.527 \pm 0.030) \times 10^{-5}$. The
128 quoted errors on $(D/H)_{\text{BBN}}$ stem from the propagation of uncertainties in the baryon density (first
129 error) and the nuclear rates (second error).

130 To probe the existence of physics beyond the Λ CDM model, we performed likelihood analy-
131 ses in which both $\Omega_b h^2$ and N_{eff} were left as free parameters. Since the deuterium abundance alone
132 cannot be used to constrain $\Omega_b h^2$ and N_{eff} when they are both varied, we considered two cases
133 with additional inputs. In one case, hereafter (D+CMB), we used the deuterium abundance, both
134 observed $(D/H)_{\text{obs}}$ and predicted $(D/H)_{\text{BBN}}$, combined with a Gaussian distribution of the CMB
135 baryon density⁷, with mean value and uncertainty as obtained by PLANCK without constraining
136 N_{eff} ; in the second case, hereafter (D+ Y_p), we used observed and predicted values of both the deu-
137 terium abundance and the ${}^4\text{He}$ mass fraction²⁵, Y_p , without constraining $\Omega_b h^2$. Results are shown
138 in Figure 3 as contour plots in the plane N_{eff} vs. $\Omega_b h^2$. Numerical values at 68% confidence level
139 are reported in Table 1. We note that, at the 99% confidence level, we obtain $N_{\text{eff}} = 2.95^{+0.61}_{-0.57}$
140 and $N_{\text{eff}} = 2.86^{+0.75}_{-0.67}$ for the two (D+CMB) and (D+ Y_p) cases, respectively. Our largest values of
141 N_{eff} deviate by at most 20% from its standard value^{23,24} $N_{\text{eff}} = 3.045$. This implies a maximum
142 amount of “dark radiation”, due to particle species which are not foreseen by the standard model
143 of particle physics, in agreement with PLANCK⁷.

144 Although the (D+CMB) and (D+ Y_p) cases discussed above lead to consistent outcomes,
145 the (D+ Y_p) result depends on the value of Y_p used. In our analysis, we adopted the value of
146 Aver *et al.*²⁵, which is close to those of Peimbert *et al.*²⁶, Valerdi *et al.*²⁷, and the recommended
147 value in Tanabashi *et al.*². When the much higher Y_p value of Izotov *et al.*²⁸ is used, we obtain
148 $N_{\text{eff}} = 3.60_{-0.43}^{+0.45}$ (99% confidence level).

149 To conclude, we have measured the $D(p,\gamma)^3\text{He}$ reaction cross section to an unprecedented
150 precision of better than 3% by exploiting the million-fold reduction in cosmic-ray muons at LUNA.
151 The new S factor has led to a remarkable improvement in the evaluation of the present-day baryon
152 density, $\Omega_b h^2$, using standard Big Bang Nucleosynthesis alone. Our value is now in better agree-
153 ment with the one derived from the analysis of the Cosmic Microwave Background anisotropies
154 and provides further support to the standard cosmological model. When combined with additional
155 inputs such as CMB baryon density or the primordial helium abundance, our data also provide a
156 strong experimental foundation to constrain the amount of dark radiation.

157 **Methods**

158 **D(p, γ)³He cross-section measurements at LUNA.** The cross section of the D(p, γ)³He reaction
159 ($Q = 5.493$ MeV) was measured in direct kinematics using a high intensity (100 – 300 μ A) proton
160 beam from the LUNA-400kV accelerator¹¹ over the full dynamic energy range $E_p = 50 - 395$ keV,
161 corresponding to centre-of-mass energies $E = 33 - 263$ keV. The beam was sent onto a windowless
162 and extended gas target containing high-purity (99.999%) deuterium maintained at a pressure of
163 $P = 0.3$ mbar by a system of three differential pumping stages. A copper calorimeter²⁹ at the end
164 of the gas target stopped the beam and allowed its intensity to be measured. Gamma rays from
165 the D(p, γ)³He reaction were detected by a large high-purity germanium detector (HPGe) mounted
166 in close geometry under the target chamber and facing its centre. Full details of the experimental
167 setup and its commissioning have been described elsewhere¹⁰.

168 For an extended gas target of length L , the cross section of the D(p, γ)³He reaction can be
169 expressed in terms of experimentally measurable quantities as:

$$\sigma(E) = \frac{N_\gamma(E)}{N_p \int_0^L \rho(z) \epsilon(z, E_\gamma) W(z) dz} \quad (1)$$

170 where $N_\gamma(E)$ is the net number of detected γ rays at a given interaction energy E , N_p is the number
171 of incident protons, $\rho(z)$ is the number density of target atoms as a function of interaction position
172 z along the target, $\epsilon(z, E_\gamma)$ is the γ -ray detection efficiency, and $W(z)$ is a term accounting for the
173 angular distribution of the emitted γ rays.

174 Under experimental conditions at LUNA, the γ rays emitted by the D(p, γ)³He reaction
175 ($Q = 5.5$ MeV) have energies $E_\gamma = 5.5 - 5.8$ MeV, *i.e.* far away from the energy of the com-

176 monly used radioactive sources. Thus, a measurement of the detection (photo-peak) efficiency was
177 performed using different-energy γ rays emitted in cascade from the well-known resonant reac-
178 tion $^{14}\text{N}(p,\gamma_1\gamma_2)^{15}\text{O}$. Efficiency corrections were validated by extensive Monte-Carlo simulations
179 as described in detail in Mossa *et al.*¹⁰.

180 To reduce the uncertainty on the final cross-section, we performed dedicated measurements
181 to minimise the systematic errors associated with each term of Eq. (1).

182 A typical γ -ray spectrum taken at a proton beam energy $E_p = 50$ keV is shown in Extended
183 Data Figure 1. We note that the γ -ray background at LUNA is 3-4 orders of magnitude lower than
184 on the Earth's surface⁸ in the region of interest ($E_\gamma \simeq 5.5 - 5.8$ MeV) for the $\text{D}(p,\gamma)^3\text{He}$ reaction.
185 As a result, the counting statistical error could be kept below 1% at all beam energies. The main
186 source of beam-induced background was due to the $^{19}\text{F}(p,\alpha\gamma)^{16}\text{O}$ reaction from the interaction
187 of protons with fluorine contaminant usually present on collimators along the gas target and on
188 the calorimeter¹⁰ (beam dump). This beam-induced background ($E_\gamma < 7$ MeV) was found to
189 be negligible at beam energies $E_p < 250$ keV. At higher energies, approaching the well-known
190 $^{19}\text{F}(p,\alpha\gamma)^{16}\text{O}$ resonance at $E_p = 340$ keV, the beam-induced background was carefully accounted
191 for in dedicated control runs in which (inert) ^4He gas was used instead of deuterium. A sample
192 spectrum taken at the highest beam energy studied ($E_p = 395$ keV) is shown in Extended Data
193 Figure 2.

194 The cross-section results obtained at LUNA for the $\text{D}(p,\gamma)^3\text{He}$ reaction are shown in Figure 1
195 (and summarised in Extended Data Table 1) in the form of the astrophysical S factor. This is

196 defined as³⁰ $S(E) = E\sigma(E) \exp(2\pi\eta)$, where E is the energy of interaction, $\sigma(E)$ is the energy
 197 dependent cross section, and η is the Sommerfeld parameter $\eta(E) = Z_1 Z_2 \alpha (\mu c^2 / 2E)^{1/2}$ (where
 198 Z_1 and Z_2 are the atomic numbers of the interacting nuclei, α is the fine structure constant, μ
 199 is the reduced mass, and c is the speed of light). We achieved an overall systematic uncertainty
 200 lower than 3%, with main contributions arising from uncertainties in beam current (1%), target
 201 density profile (1.1%), and efficiency (2%), as described in Mossa *et al.*¹⁰. We note that our new
 202 experimental data are close to a previous fit²¹ (not shown in Fig. 1) based on a Bayesian analysis
 203 of previous selected experimental data sets.

204 Our new S factor was used together with other data sets^{13–16,31–33} to arrive at the best fit:

$$S(E) = 0.2121 + 5.973 \times 10^{-3} E + 5.449 \times 10^{-6} E^2 - 1.656 \times 10^{-9} E^3 \quad [\text{eV b}] \quad (2)$$

205 (with E in keV) shown in Fig. 1 (red solid line). The fit was performed over a broad energy range
 206 $E_{\text{cm}} = 2 - 2000$ keV, following the approach of Serpico *et al.*³⁴. At BBN energies, the fit is entirely
 207 dominated by the new LUNA data reported here, thanks to their increased precision compared to
 208 previous works. We obtain a reduced χ^2 of 1.049. The uncertainties on the fit (red band in Fig. 2)
 209 are given by:

$$(\Delta S(E))^2 = 1.4 \times 10^{-5} + 2.97 \times 10^{-8} E^2 + 4.80 \times 10^{-13} E^4 + 1.12 \times 10^{-19} E^6 \quad [(\text{eV b})^2] \quad (3)$$

210 (with E in keV). The correlation among data points of the same data set was properly taken into
 211 account³⁴ by introducing a single normalization factor for each data set, constrained by the so-
 212 called penalty factor in the χ^2 .

213 As the universe expands, BBN takes place over a temperature range of the nucleon-photon

214 plasma $k_B T \sim 100 - 20$ keV, with k_B being the Boltzmann constant. To better assess the en-
 215 ergy range where precise measurements of the $D(p,\gamma)^3\text{He}$ cross section have the largest impact in
 216 improving the accuracy of theoretical predictions of primordial deuterium abundance relative to
 217 hydrogen, $(D/H)_{\text{BBN}}$, we used a *sensitivity function* (see for example Nollett *et al.*³⁵), defined as
 218 the ratio of the logarithmic derivatives of the D/H abundance and the corresponding S factor:

$$\zeta(E) = \frac{\delta \log(D/H)_{\text{BBN}}}{\delta \log S(E)} \quad (4)$$

219 Specifically, we varied the S factor in 10 keV energy bins, over a broad energy region of
 220 10 – 500 keV, and calculated the corresponding thermal rate (obtained by convolution with the
 221 Maxwell-Boltzmann distribution) bin by bin as a function of energy. The corresponding yield of
 222 deuterium was obtained using the PARthENoPE code²² (see also Methods “Bayesian Likelihood
 223 Analysis”). The results are shown in Extended Data Figure 3. We note that the sensitivity curve
 224 remains above 25% of the maximum variation in a range $E = 20 - 240$ keV, with the deuterium
 225 abundance being most sensitive to the $D(p,\gamma)^3\text{He}$ cross section at $E \simeq 80$ keV, i.e. in a region
 226 where our precision underground measurements are essential. Our values of the $D(p,\gamma)^3\text{He}$ thermal
 227 rate and their uncertainties are provided in Extended Data Table 2.

228 **Bayesian Likelihood Analysis.** To study the effect of the new LUNA $D(p,\gamma)^3\text{He}$ S factor on
 229 primordial deuterium produced during Big Bang Nucleosynthesis, we have computed the corre-
 230 sponding thermal rate and updated it (Pisanti *et al.*, in preparation) in the second release of the
 231 BBN code PARthENoPE²². The rates of the $D(d,n)^3\text{He}$ and $D(d,p)^3\text{H}$ have also been updated fol-
 232 lowing the publication of new data sets³⁶, although their inclusion has a negligible effect (Pisanti

233 *et al.*, in preparation) on the uncertainty on the $(D/H)_{\text{BBN}}$ value presented in this work. Starting
 234 from conditions of nuclear statistical equilibrium, PARthENoPE solves a set of coupled ordinary
 235 differential equations that follow the departure from chemical equilibrium of nuclear species and
 236 determines their asymptotic abundances as a function of several input cosmological parameters
 237 such as the baryon density $\Omega_b h^2$, the number of effective neutrino species N_{eff} , the value of the
 238 cosmological constant, and neutrino chemical potentials (see, e.g. Pisanti *et al.*³⁷ for details).

239 The reduced uncertainty of the LUNA results affects the precision of BBN deuterium predic-
 240 tion and can constrain the baryon density. In a first analysis we assume a standard BBN scenario
 241 and fix the value of the relativistic degrees of freedom to photons and three active neutrino species
 242 ($N_\nu = 3$) corresponding to a contribution $N_{\text{eff}} = 3.045$ in the energy density of neutrinos, conven-
 243 tionally given⁶ as $\rho_\nu = \frac{7}{8}(\frac{4}{11})^{4/3}\rho_\gamma N_{\text{eff}}$ (with ρ_γ being the photon density). We use $(D/H)_{\text{BBN}}$ as a
 244 function of $\Omega_b h^2$ and the deuterium abundance inferred from astronomical observations $(D/H)_{\text{obs}}$.
 245 The likelihood function is:

$$\mathcal{L}_{D+3\nu}(\Omega_b h^2) = \exp \left[-\frac{[(D/H)_{\text{BBN}}(\Omega_b h^2) - (D/H)_{\text{obs}}]^2}{2[\sigma_{\text{BBN}}^2(\Omega_b h^2) + \sigma_{\text{obs}}^2]} \right] \quad (5)$$

246 where σ_{BBN} is the propagated error on the deuterium yield due to the experimental uncertainties
 247 on nuclear reactions, and σ_{obs} is the uncertainty on the astronomical observations.

248 We performed two other analyses in which both $\Omega_b h^2$ and N_{eff} were free to vary and con-
 249 strained the likelihood function $\mathcal{L}_{\text{D}}(\Omega_b h^2, N_{\text{eff}})$ with other astrophysical inputs. In one case,
 250 (D+CMB), we used the deuterium abundance (both predicted and observed) and assumed a Gaus-
 251 sian distribution on the baryon density, $\mathcal{L}_{\text{CMB}}(\Omega_b h^2)$, corresponding to the latest PLANCK value⁷

252 $\Omega_b h^2(\text{CMB}) = 0.02224 \pm 0.00022$, obtained without constraining N_{eff} . The likelihood function is
 253 now expressed as:

$$\mathcal{L}_{\text{D+CMB}}(\Omega_b h^2, N_{\text{eff}}) = \mathcal{L}_{\text{CMB}}(\Omega_b h^2) \exp \left[-\frac{[(\text{D}/\text{H})_{\text{BBN}}(\Omega_b h^2, N_{\text{eff}}) - (\text{D}/\text{H})_{\text{obs}}]^2}{2[\sigma_{\text{BBN}}^2(\Omega_b h^2, N_{\text{eff}}) + \sigma_{\text{obs}}^2]} \right] \quad (6)$$

254 In the other case, $(\text{D}+Y_p)$, we used BBN predictions and observed abundances of both deu-
 255 terium and ${}^4\text{He}$ mass fraction ($Y_p = 0.2449 \pm 0.0040$ from astronomical observations²⁵) together
 256 with the most recent² neutron lifetime ($\tau_n = 879.4 \pm 0.6$ s), which carries the largest uncertainty on
 257 the theoretical prediction of ${}^4\text{He}$ primordial abundance. No prior distribution was assumed on the
 258 baryon density. In this case, the likelihood function is the product of two exponential functions:
 259 one for deuterium as that appearing in Eq. (6) and a similar one for ${}^4\text{He}$.

- 260 1. Cyburt, R. H., Fields, B. D., Olive, K. A. & Yeh, T.-H. Big bang nucleosynthesis: Present
 262 status. *Rev. Mod. Phys.* **88**, 015004 (2016).
- 263 2. Tanabashi, M. *et al.*. Review of Particle Physics. *Phys. Rev. D* **830**, 030001 (2018, and 2019
 264 update).
- 265 3. Cooke, R., Pettini, M. & Steidel, C. One Percent Determination of the Primordial Deuterium
 266 Abundance. *Astrophys. J.* **855**, 102 (2018).
- 267 4. Pitrou, C., Coc, A., Uzan, J. & Vangioni, E. Precision big bang nucleosynthesis with improved
 268 Helium-4 predictions. *Phys. Rep.* **754**, 1–66 (2018).
- 269 5. Coc, A. *et al.* New reaction rates for improved primordial D/H calculation and the cosmic
 270 evolution of deuterium. *Phys. Rev. D* **92**, 123526 (2015).

- 271 6. Di Valentino, E. *et al.* Probing nuclear rates with Planck and BICEP2. *Phys. Rev. D* **90**, 023543
272 (2014).
- 273 7. Aghanim, N. *et al.* Planck 2018 results. VI. Cosmological parameters. *arXiv e-prints*
274 arXiv:1807.06209 (2018).
- 275 8. Brogini, C., Bemmerer, D., Caciolli, A. & Trezzi, D. Luna: Status and prospects.
276 *Prog. Part. Nucl. Phys.* **98**, 55–84 (2018).
- 277 9. Cavanna, F. & Prati, P. Direct measurement of nuclear cross-section of astrophysical interest:
278 Results and perspectives. *Int. J. Mod. Phys. A* **33**, 1843010–346 (2018).
- 279 10. Mossa, V. *et al.*. Setup commissioning for an improved measurement of the $D(p,\gamma)^3\text{He}$ cross
280 section at Big Bang Nucleosynthesis energies. *Eur. Phys. J. A* **56**, 144 (2020).
- 281 11. Formicola, A. *et al.* The LUNA II 400kV accelerator. *Nucl. Inst. Meth. A* **507**, 609–616
282 (2003).
- 283 12. Fields, B. D., Olive, K. A., Yeh, T.-H. & Young, C. Big-Bang Nucleosynthesis after Planck.
284 *Journ. Cosm. and Astropart. Phys.* **2020**, 010–010 (2020).
- 285 13. Casella, C. *et al.* First measurement of the $d(p,\gamma)^3\text{He}$ cross section down to the solar Gamow
286 peak. *Nucl. Phys. A* **706**, 203–216 (2002).
- 287 14. Ma, L. *et al.* Measurements of $^1\text{H}(d,\gamma)^3\text{He}$ and $^2\text{H}(p,\gamma)^3\text{He}$ at very low energies. *Phys. Rev. C*
288 **55**, 588–596 (1997).

- 289 15. Griffiths, G., Larson, E. & Robertson, L. The capture of protons by deuterons. *Can. J. Phys.*
290 **40**, 402 (1962).
- 291 16. Schmid, G. *et al.* The ${}^2\text{H}(p,\gamma){}^3\text{He}$ and ${}^1\text{H}(d,\gamma){}^3\text{He}$ reactions below 80 keV. *Phys. Rev. C* **56**,
292 2565–2581 (1997).
- 293 17. Tišma, I. *et al.* Experimental cross section and angular distribution of the ${}^2\text{H}(p,\gamma){}^3\text{He}$ reaction
294 at Big-Bang nucleosynthesis energies. *Eur. Phys. J. A* **55**, 137 (2019).
- 295 18. Marcucci, L., Mangano, G., Kievsky, A. & Viviani, M. Implication of the Proton-Deuteron
296 Radiative Capture for Big Bang Nucleosynthesis. *Phys. Rev. Lett.* **116**, 102501 (2016).
- 297 19. Adelberger, E. *et al.* Solar fusion cross sections. II. The pp chain and CNO cycles.
298 *Rev. Mod. Phys.* **83**, 195–246 (2011).
- 299 20. Schmid, G. *et al.*. Effects of Non-nucleonic Degrees of Freedom in the $D(\vec{p},\gamma){}^3\text{He}$ and the
300 $p(\vec{d},\gamma){}^3\text{He}$ reactions. *Phys. Rev. Lett.* **76**, 3088 (1996).
- 301 21. Iliadis, C., Anderson, K. S., Coc, A., Timmes, F. X. & Starrfield, S. BAYESIAN ESTIMA-
302 TION OF THERMONUCLEAR REACTION RATES. *Astrophys. J.* **831**, 107 (2016).
- 303 22. Consiglio, R. *et al.* PARthENoPE reloaded. *Comp. Phys. Comm.* **233**, 237 (2018).
- 304 23. De Salas, P. & Pastor, S. Relic neutrino decoupling with flavour oscillations revisited. *Journ.*
305 *Cosm. and Astropart. Phys.* **07**, 051 (2016).
- 306 24. Mangano, G. *et al.* Relic neutrino decoupling including flavour oscillations. *Nucl. Phys. B*
307 **729**, 221 (2005).

- 308 25. Aver, E., Olive, K. A., & Skillman, E. D. The effects of He I λ 10830 on helium abundance
309 determinations. *Journ. Cosm. and Astropart. Phys.* **07**, 011 (2015).
- 310 26. Peimbert, A., Peimbert, M. & Luridiana, V. The primordial helium abundance and the number
311 of neutrino families. *Rev. Mex. Astron. Astrofis.* **52**, 419 (2016).
- 312 27. Valerdi, M., Peimbert, A., Peimbert, M. & Sixtos, A. Determination of the primordial helium
313 abundance based on NGC 346, an h ii region of the small magellanic cloud. *Astrophys. J.* **876**,
314 98 (2019).
- 315 28. Izotov, Y. I., Thuan, T. X. & Guseva, N. G. The primordial deuterium abundance of the most
316 metal-poor damped Ly α system. *M.N.R.A.S.* **445**, 778 (2014).
- 317 29. Ferraro, F. *et al.* A high-efficiency gas target setup for underground experiments, and redeter-
318 mination of the branching ratio of the 189.5 keV $^{22}\text{Ne}(p,\gamma)^{23}\text{Na}$ resonance. *Eur. Phys. J. A* **54**,
319 44 (2018).
- 320 30. Rolfs, C. & Rodney, W. *Cauldrons in the Cosmos* (University of Chicago Press, Chicago,
321 1988).
- 322 31. Griffiths, G., Lal, M. & Scarfe, C. The reaction $\text{D}(p,\gamma)^3\text{He}$ below 50 keV. *Can. J. Phys.* **41**,
323 724 (1963).
- 324 32. Warren, J. B., Erdman, K. L., Robertson, L. P., Axen, D. A. & Macdonald, J. R. Photodisinte-
325 gration of ^3He near the threshold. *Phys. Rev.* **132**, 1691–1692 (1963).

- 326 33. Geller, K., Muirhead, E. & Cohen, L. The ${}^2\text{h}(p,\gamma){}^3\text{he}$ reaction at the breakup threshold. *Nu-*
327 *clear Physics A* **96**, 397 – 400 (1967).
- 328 34. Serpico, P. D. *et al.* Nuclear reaction network for primordial nucleosynthesis: a detailed
329 analysis of rates, uncertainties and light nuclei yields. *Journ. Cosm. and Astropart. Phys.*
330 **2004**, 010–010 (2004).
- 331 35. Nollett, K. M. & Burles, S. Estimating reaction rates and uncertainties for primordial nucle-
332 osynthesis. *Phys. Rev. D* **61**, 123505 (2000).
- 333 36. Tumino, A. *et al.* New determination of the ${}^2\text{H}(d,p){}^3\text{H}$ and ${}^2\text{H}(d,n){}^3\text{He}$ reaction rates at astro-
334 physical energies. *Astrophys. J.* **785**, 96 (2014).
- 335 37. Pisanti, O. *et al.* PArthENoPE: Public algorithm evaluating the nucleosynthesis of primordial
336 elements. *Comp. Phys. Comm.* **178**, 956–971 (2008).

337 **Acknowledgements** We thank Donatello Cicotti for accelerator operation and maintance, for mechani-
338 cal setups and servicing of the vacuum systems during the course of the experiment, Marco D’Incecco for
339 work on custom electronics, Massimiliano De Deo for the data acquisition system, and Giuliano Sobrero
340 for a new gas target control panel. We also thank the mechanical workshop at LNGS, INFN Bari and Di-
341 partimento Interateneo di Fisica Bari. This work was supported by INFN, with contributions from DFG
342 (BE4100/4-1), Helmholtz Association (ERC-RA-0016), NKFIH (K120666), COST Association (ChETEC
343 CA16117), STFC-UK, University of Naples Compagnia di San Paolo grant STAR, the research grant num-
344 ber 2017W4HA7S NAT-NET: “Neutrino and Astroparticle Theory Network” under the program PRIN 2017
345 funded by the Italian Ministero dell’Istruzione, dell’Università della Ricerca (MIUR), and INFN Iniziativa

346 Specifica TAsP. R.D. acknowledges funding from Italian Ministry of Education, University and Research
347 (MIUR) through the “Dipartimenti di eccellenza” project Science of the Universe.

348 **Author Contributions** The experiment at LUNA was proposed by CG and coordinated by FC and DT.
349 PC, CG, SZ and VM planned the setup; SZ and PC developed the Monte Carlo simulations; SZ, FC, PC,
350 CG, VM, KS and FF led the data analysis. Other authors contributed to the data taking over a period of 2
351 years and to discussion and interpretation of the results obtained. MJ also has overall responsibility for the
352 accelerator operations and the underground site. GM and OP performed all BBN calculations and Bayesian
353 analyses. LEM, AK, MV performed *ab-initio* calculations. MA, FC, CG, GM and OP also wrote the paper.

354 **Competing interests** The authors declare no competing financial interests.

355 **Data availability** Experimental data taken at LUNA are proprietary to the Collaboration but can be made
356 available from the corresponding authors upon reasonable request. Values of the thermonuclear reaction rate
357 for smaller temperature steps can be obtained upon request to O.P.

358 **Code availability** The PArthENoPE code used for BBN calculations can be made available upon request
359 to O.P.

360 **Correspondence** Correspondence and requests for materials should be addressed to C.G. and S.Z. (email:
361 carlo.gustavino@roma1.infn.it and sandra.zavatarelli@ge.infn.it).

Table 1: **Mean values and 68% confidence-level ranges for the baryon density $\Omega_b h^2$ (with relative uncertainties δ) and the effective number of neutrino species N_{eff} .** The first two lines show the results obtained from the likelihood analyses performed in this study, without and with the new $D(p,\gamma)^3\text{He}$ S factor obtained at LUNA and with N_{eff} fixed to its standard value^{23,24} of 3.045. The third and fourth lines show results obtained, respectively, using CMB data alone¹² (CMB+ 3ν) and CMB data combined with the theoretical dependence of primordial ^4He on baryon density⁷ (PLANCK+ 3ν). The last two lines correspond to cases in which both $\Omega_b h^2$ and N_{eff} are left as free parameters and the likelihood functions are constrained by either the deuterium abundance and a prior distribution on $\Omega_b h^2$, (D+CMB) case, or the observed and predicted abundances of both deuterium and helium, (D+ Y_p) case (in both cases the predicted deuterium abundance takes into account our new LUNA results; see Methods for details).

	$\Omega_b h^2$	δ [%]	N_{eff}
D+ 3ν (without LUNA data)	0.02271 ± 0.00062	2.73	3.045
D+ 3ν (with new LUNA data)	0.02233 ± 0.00036	1.61	3.045
CMB+ 3ν	$0.02230 \pm 0.00021^a)$	0.94	3.045
PLANCK+ 3ν	0.02236 ± 0.00015	0.67	3.045
D+CMB	0.02224 ± 0.00022	0.99	2.95 ± 0.22
D+ Y_p	0.0221 ± 0.0006	2.71	$2.86^{+0.28}_{-0.27}$

^{a)}Quoted in Fields *et al.*¹² as 0.022298 ± 0.000214 .

Extended Data Table 1: **Astrophysical S factors for the $D(p,\gamma)^3\text{He}$ reaction at the measured centre-of-mass energies.** Values of the astrophysical S factor as measured at LUNA over the full energy range explored. Statistical (σ_{stat}) and systematic (σ_{sys}) uncertainties at 68% confidence level are also reported. The statistical uncertainty is typically negligible except at the lowest energy point (3.6%), where it dominates over the systematic uncertainty (2.7%). Systematic uncertainties remain below 3% at all energies.

E [keV]	$S(E)$ [eV b]	σ_{stat} [eV b]	σ_{sys} [eV b]
32.4	0.386	0.014	0.010
66.7	0.627	0.009	0.016
99.5	0.850	0.008	0.021
115.9	0.966	0.009	0.024
132.9	1.133	0.004	0.031
149.3	1.223	0.006	0.031
166.1	1.375	0.004	0.036
182.7	1.475	0.006	0.037
199.5	1.648	0.003	0.043
222.8	1.791	0.006	0.045
232.9	1.866	0.012	0.051
252.9	2.073	0.012	0.052
262.9	2.156	0.020	0.054

Extended Data Table 2: **Thermonuclear reaction rate for the $D(p,\gamma)^3\text{He}$ reaction.** Values of the thermonuclear reaction rate R obtained from our best fit S factor of the $D(p,\gamma)^3\text{He}$ reaction as a function of temperature in GK. Low- and high-rates are quoted at the 1σ level.

T [GK]	R [$\text{cm}^3\text{mol}^{-1}\text{s}^{-1}$]	R_{low} [$\text{cm}^3\text{mol}^{-1}\text{s}^{-1}$]	R_{high} [$\text{cm}^3\text{mol}^{-1}\text{s}^{-1}$]
0.001	1.37×10^{-11}	1.35×10^{-11}	1.39×10^{-11}
0.005	2.57×10^{-5}	2.53×10^{-5}	2.62×10^{-5}
0.01	1.53×10^{-3}	1.51×10^{-3}	1.56×10^{-3}
0.05	9.08×10^{-1}	8.94×10^{-1}	9.22×10^{-1}
0.10	5.74×10^0	5.65×10^0	5.84×10^0
0.50	1.29×10^2	1.26×10^2	1.32×10^2
1.0	3.63×10^2	3.52×10^2	3.74×10^2
1.5	6.32×10^2	6.09×10^2	6.56×10^2
2.0	9.20×10^2	8.79×10^2	9.62×10^2
3.0	1.52×10^3	1.43×10^3	1.61×10^3
4.0	2.11×10^3	1.95×10^3	2.28×10^3
5.0	2.67×10^3	2.40×10^3	2.93×10^3
6.0	3.16×10^3	2.76×10^3	3.55×10^3
7.0	3.56×10^3	3.00×10^3	4.12×10^3
8.0	3.85×10^3	3.09×10^3	4.61×10^3
9.0	4.01×10^3	3.02×10^3	5.01×10^3
10.0	4.02×10^3	2.75×10^3	5.30×10^3

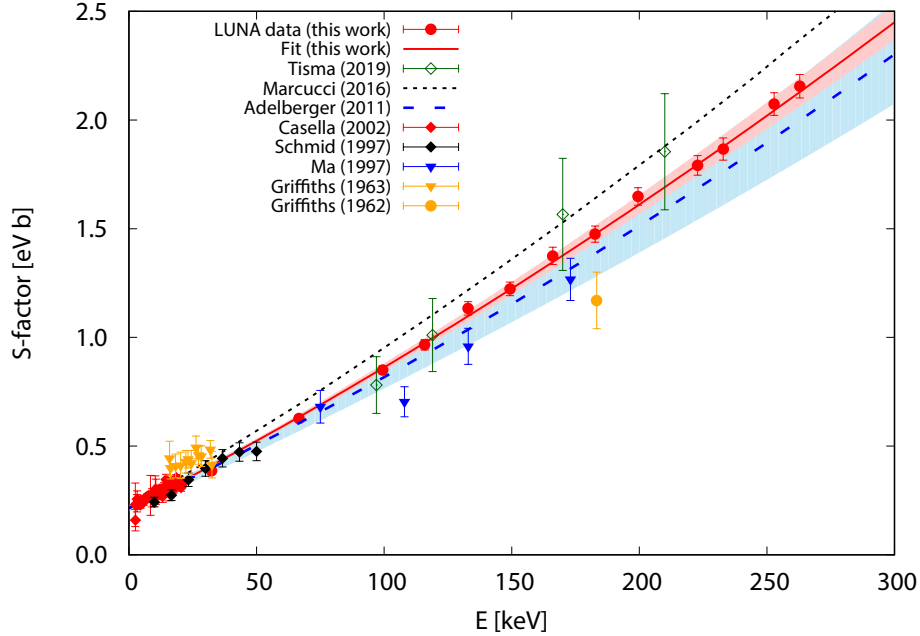


Figure 1: **S factor of the $D(p,\gamma)^3\text{He}$ reaction.** At BBN energies ($E_{\text{cm}} \simeq 30 - 300$ keV), the new LUNA results (filled red circles) indicate a faster deuterium destruction compared to a best fit¹⁹ (blue dashed line) of previous experimental data, but a slower destruction compared to theoretical calculations¹⁸ (black dotted line). At BBN energies, the best fit (red solid line, Eq. 2) obtained in this work is entirely dominated by the LUNA data. The fit includes all experimental data^{13–16,31–33} (note that those by Warren *et al.*³² and Geller *et al.*³³ lie outside the energy range shown here). Bands represent the 68% confidence level.

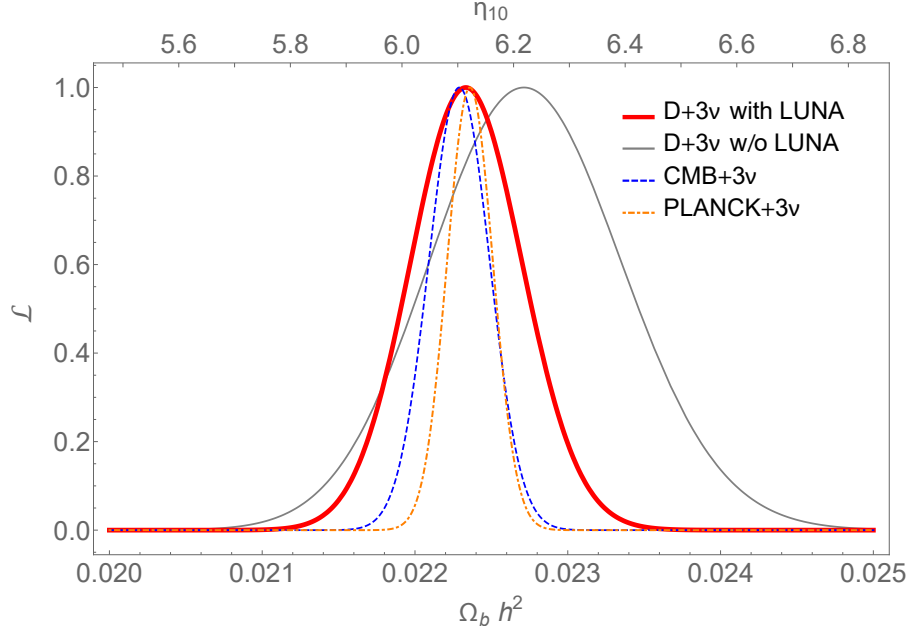


Figure 2: **Likelihood distribution of the baryon density (lower x -axis) and baryon-to-photon ratio (η_{10} , upper x -axis).** The red curve (D+3 ν with LUNA) shows the distribution of the baryon density obtained using the new LUNA S factor for the predicted deuterium abundance $(D/H)_{\text{BBN}}$. Note the factor of 2 reduction in the uncertainty, as compared to the distribution based on previous S factor¹⁹ (grey curve, D+3 ν w/o LUNA). Our new determination of $\Omega_b h^2$ is now in much better agreement with the value obtained from CMB data alone¹² (blue dashed curve, CMB+3 ν) and with the best determination of baryon density obtained by PLANCK⁷ from CMB data combined with additional observational inputs and with the theoretical dependence of primordial ${}^4\text{He}$ on baryon density (orange dot-dashed curve, PLANCK+3 ν).

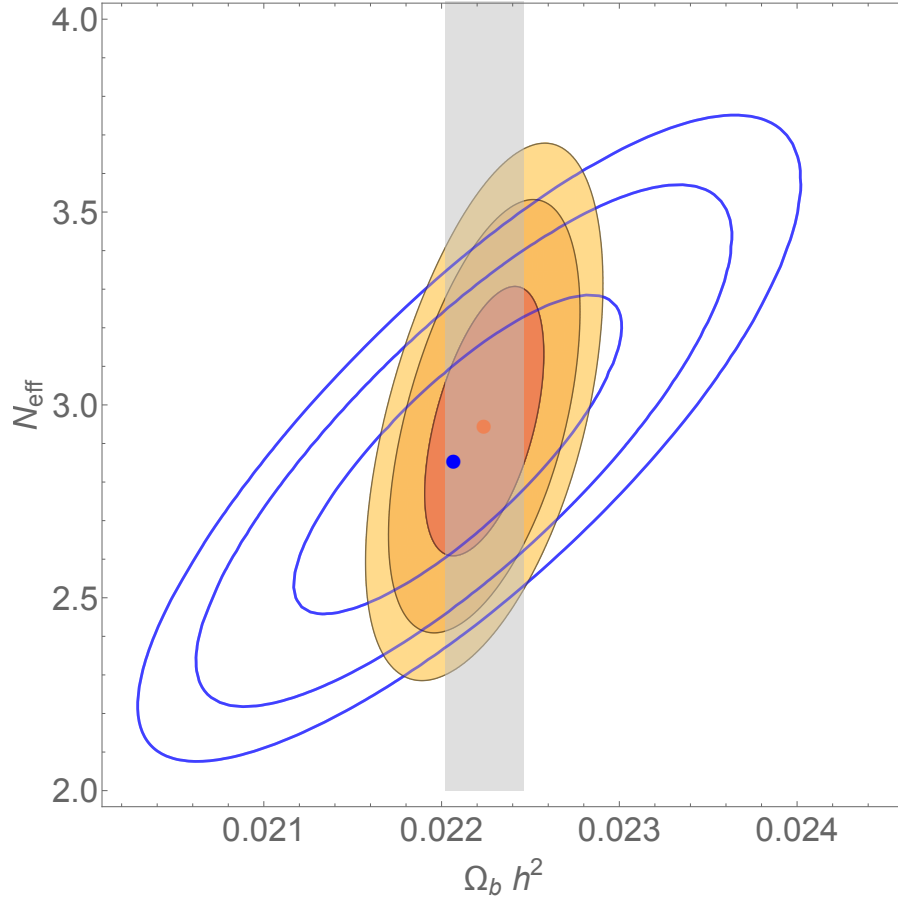
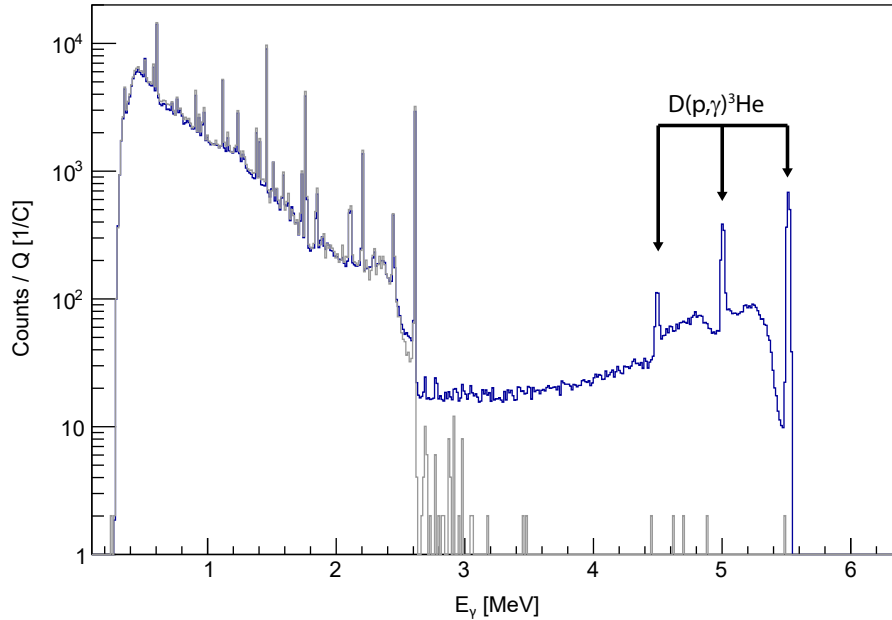
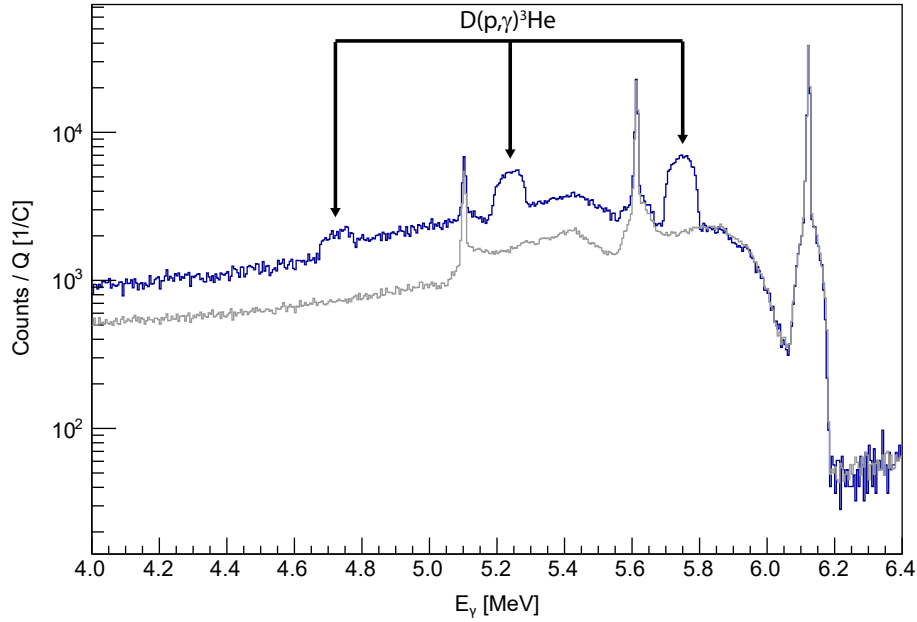


Figure 3: **Likelihood contours (at 68%, 95% and 99% confidence level) on the N_{eff} vs. $\Omega_b h^2$ plane.** Orange filled contours are obtained for the D+CMB case using the observed deuterium abundance³ $(D/H)_{\text{obs}}$ and the adopted PLANCK distribution on baryon density⁷ (grey vertical band at the 68% confidence level). Blue contours correspond to the D+ Y_p case, as obtained from a likelihood analysis with observed abundances of deuterium³ and ${}^4\text{He}$ mass fraction²⁵, Y_p , and the corresponding BBN theoretical predictions (see Methods for details). Central values for each case are indicated by dots.

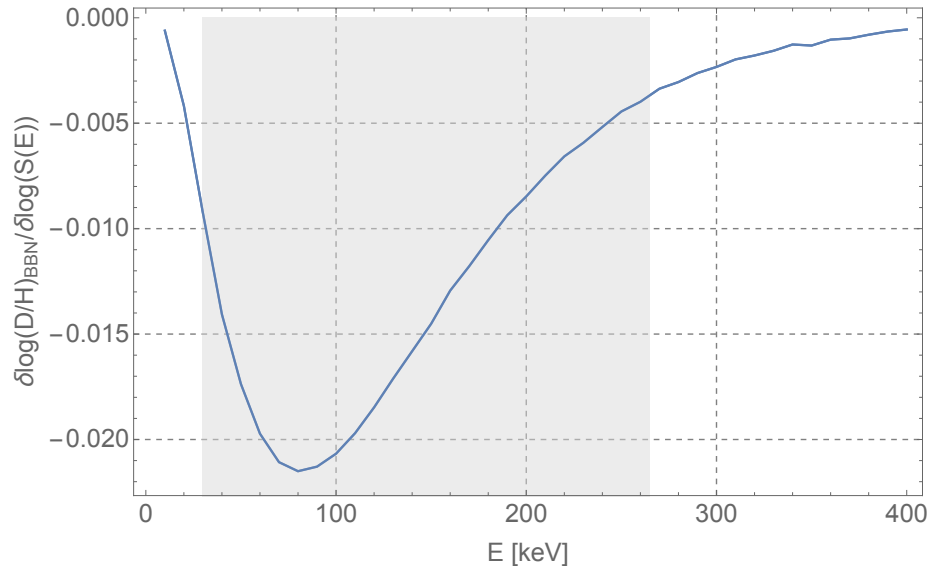


Extended Data Figure 1: **Typical γ -ray spectrum obtained underground with the HPGe detector at proton beam energy $E_p = 50$ keV.** Typical γ -ray spectrum (blue) obtained with the deuterium gas target at $P = 0.3$ mbar, clearly showing the full-energy, single- and double-escape peaks from the $D(p,\gamma)^3\text{He}$ reaction. The continuum is mainly due to Compton scattering events in which photons deposit only part of their energy in the detector. In grey is the beam-induced background spectrum acquired in the control run under the same experimental conditions but with an inert ^4He gas target. Both spectra are normalised to the integrated beam current. The region of interest ($E_\gamma \sim 4.5 - 5.8$ MeV) is essentially background free thanks to the million-fold shielding⁸ from cosmic-ray muons obtained at the LUNA underground laboratory.



Extended Data Figure 2: **Typical γ -ray spectrum taken at proton beam energy $E_p = 395$ keV.**

In blue, γ -ray spectrum obtained with the deuterium gas target at $P = 0.3$ mbar (the peaks from the $D(p,\gamma)^3\text{He}$ reaction are broadened by the Doppler effect at this higher beam energy). In grey, beam-induced background spectrum (acquired with an inert ^4He gas target) due to the ^{19}F contaminant (see text). Its contribution was subtracted leading to net counts on the full energy peak with a statistical uncertainty of 0.9%. Both spectra are normalised to the integrated beam current.



Extended Data Figure 3: **Sensitivity of the primordial deuterium abundance to the $D(p,\gamma)^3\text{He}$ reaction cross section as a function of centre-of-mass energy.** The greatest sensitivity is obtained around $E = 80$ keV, where underground measurements are especially effective. The grey area represents the energy region explored at LUNA (see Methods for details).